Numerical Analysis of a $LiFePO_4$/Graphite Lithium-ion Coin-cell Battery

Lizhu Tong
Keisoku Engineering System Co., Ltd.
1-9-5 Uchikanda, Chiyoda-ku, Tokyo 101-0047, Japan, tong@kesco.co.jp

Abstract:
Lithium-ion batteries, based on the $LiFePO_4$/ graphite chemistry, attracts nowadays much attention for application in electric vehicles due to the excellent cycling stability of the $LiFePO_4$ electrode. In this work, we present a simulation research based on a two-dimensional axis-symmetric model of $LiFePO_4$/graphite lithium-ion batteries using COMSOL Multiphysics@. The spatial distributions of lithium ion concentration, potential and lithium concentration at the electrode particles are obtained. The electrode reaction, discharge characteristics, and the effect of electrode configuration are analyzed.

Keywords: Lithium-ion batteries, $LiFePO_4$ (LFP) cathode, Battery discharge characteristics, Numerical simulation.

1. Introduction

Electric vehicles (EVs) powered by rechargeable lithium-ion batteries (LIBs) have been developed as a replacement for the conventional internal-combustion-engine auto-mobiles. Research has been yielding a stream of improvements to the traditional LIB technology, focusing on energy and power density, durability, cost and safety [1-3]. $LiCoO_2$ (LCO), which is widely used as a cathode material for lithium-ion batteries, is now being faced to a difficulty in the application for electric vehicles due to its thermal runaway problem as well as high raw material price and resource restrictions [4,5]. $LiFePO_4$ (LFP) is a favorable choice as a cathode material in EV applications due to its stable and safe olivine structure as well as low cost, environmentally benign chemistry, and abundant iron materials as resources [6-9]. To improve its material performance, researchers have been working to overcome two major limitations of $LiFePO_4$: low electrical conductivity and small Li-ion diffusivity. The surface coating and the effect of various dopants such as metal ions on the electronic conductivity have been studied. However, it is still unclear whether the conductivity enhancement is truly intrinsic [10]. A thorough understanding of the properties of $LiFePO_4$ cathode used in lithium-ion batteries is necessary.

In this work, a $LiFePO_4$/Graphite lithium-ion battery (LIB) sealed in a CR2032-type coin cell is numerically analyzed. The finite-element analysis tool COMSOL Multiphysics@ is used in this work. Results are compared with those from the $LiCoO_2$ and $LiMn_2O_4$ cathodes.

2. Numerical Model

The LFP and graphite electrodes with 200 μm thickness used in this study are assembled and sealed in a CR2032-type coin cell, which has been used in many investigations [11-13]. The positive and negative electrodes are separated by a poly-propylene separator with 200 μm thickness. The two stainless steel spacers are used between the electrodes and coin cell case and a gasket is used to seal the coin cell. The electrolyte is a liquid electrolyte composed of 1.2 M $LiPF_6$ in 3:7 EC/ EMC solution. The mathematical equations that describe the discharge process of the coin cell have been presented in the earlier literature [14]. Briefly, these consist of a mass balance, and current conservation in the electrolyte, current conservation in the electrodes, the Butler-Volmer equation, and a charge balance relating the reaction current to the solution current.

The main electrochemical reactions of $LiFePO_4$/graphite LIBs can be represented by

$$C_6 + xLi^+ + xe^- \leftrightarrow Li_xC_6\,, \quad (1)$$

$$Li_{1-x}FePO_4 + xLi^+ + xe^- \leftrightarrow LiFePO_4. \quad (2)$$

In this work, the reactions shown in eqs. (1) and (2) are assumed to be insertion reactions occurring at the surface of small solid spherical particles of radius r_p in the electrodes. The insertion reaction is described as

$$Li^+ + e^- + \Theta_s \leftrightarrow Li\Theta_s, \quad (3)$$

where Θ_s denotes a free reaction site and $Li\Theta_s$ is an occupied reaction site at the solid particle surface. The electrochemical reactions are considered as a function of the exchange current

density and overpotential. The reaction kinetics is solved by using a Butler-Volmer expression [15]

$$i_{\text{loc}} = i_0 \left[\exp\left(\frac{\alpha_a F\eta}{RT}\right) - \exp\left(\frac{-\alpha_c F\eta}{RT}\right)\right], \quad (4)$$

$$i_0 = F(k_c)^{\alpha_a}(k_a)^{\alpha_c}(c_{s,\max} - c_s)^{\alpha_a}(c_s)^{\alpha_c} \cdot \left(c_l/c_{l,\text{ref}}\right)^{\alpha_a}, \quad (5)$$

where i_{loc} denotes the local charge transfer current density, i_0 is the exchange current density, α_a is the anodic transfer coefficient, α_c is the cathodic charge transfer coefficient, k_a is the anodic rate constant, k_c is the cathodic rate constant, η is overpotential, F is Faraday's constant, and R is the universal gas constant. c_l denotes the electrolyte salt concentration and $c_{l,\text{ref}}$ is the electrolyte reference concentration. c_s denotes the concentration of lithium ($\text{Li}\Theta_s$) in the electrode particles, $c_{s,\max}$ is the total concentration of reaction sites, and the state-of-charge variable SOC can be defined by $\text{SOC} = c_s/c_{s,\max}$.

The equilibrium potential E_{eq} of lithium insertion electrode reactions is a function of SOC, which is used to obtain the overpotential η as follows

$$\eta = \phi_s - \phi_l - E_{\text{eq}}, \quad (6)$$

where ϕ_s is the electric potential in the electrode and ϕ_l is the electrolyte potential.

Base on the electrode reaction occurred on the surface of electrode particles, lithium diffuses to and from the particle surface. The mass balance of lithium in the particles described in eq. (7) is solved in a 1D pseudo dimension [15].

$$\partial c_s/\partial t = -\nabla \cdot (-D_s \nabla c_s), \quad (7)$$

where D_s is the diffusion coefficient, and c_s is considered as an independent variable.

In this work, we focus our attention on the discharge characteristics of a coin cell battery with LFP cathode. The modeling of the two-phase process [8] of lithium insertion/deinsertion at the electrode particles in LFP is not included.

3. Simulation results

3.1 Discharge characteristics of $LiFePO_4$ (LFP) /graphite coin cells

The calculations are performed at the discharge rates of 1/2, 2/3, 1 and 3/2 C. The battery is discharged down to 2.5 V from full-charge state. The ODE Events (*ev*) interface of COMSOL Multiphysics is used to control the end of discharge. The initial state-of-charge (SOC) of LFP is 0.23, which is ~1/4 of the total concentration of reaction sites, $c_{s,\max}$ of LFP. $c_{s,\max}$=0.98 is used in this work. Figure 1 shows the distributions of electrolyte salt concentration, lithium concentration at the surface of electrode particles, and electrolyte potential at the end of discharge (C-rate=0.5) for a $LiFePO_4$/graphite cell. Due to the difference of the lengths of positive and negative electrodes, the electrolyte salt concentration and lithium concentration in the electrodes appear a large gradient at the right end close to the gasket. The temporal evolutions of cell voltage and average SOCs in the electrodes are shown in Fig. 2. At the lower discharge rates, the cell voltage smoothly decreases to 3.1 V and then quickly goes down. Since the capacity of graphite electrode is higher than that of LFP, the average SOC of graphite electrode decreases from 0.68, corresponding the full charge of LFP.

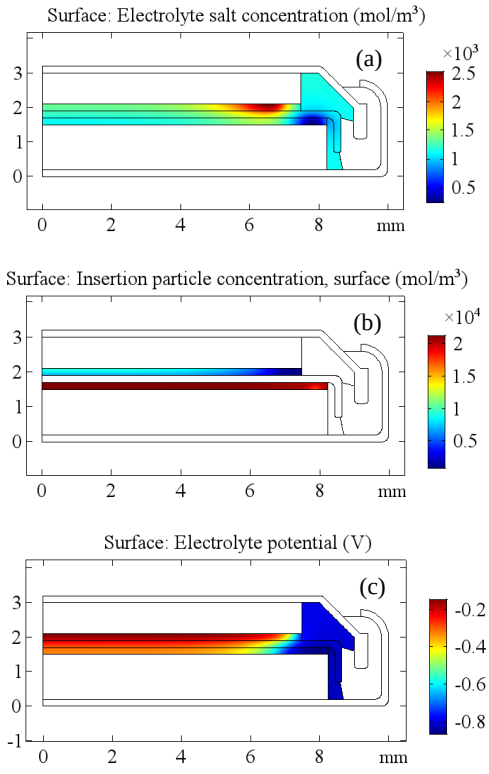

Figure 1. Calculation results of (a) electrolyte salt concentration, (b) lithium concentration at the surface of electrode particles, and (c) electrolyte potential at the end of discharge (C-rate=0.5) for a $LiFePO_4$/graphite cell.

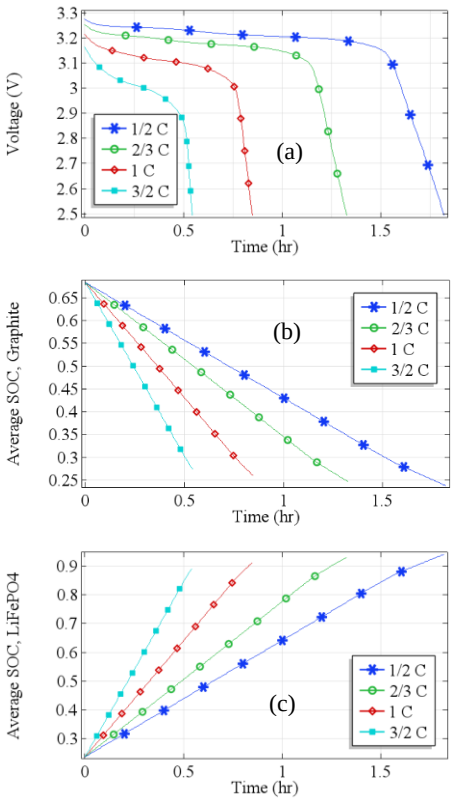

Figure 2. Temporal evolutions of (a) cell voltage, (b) average SOC in graphite electrode, and (c) average SOC in $LiFePO_4$ electrode during the discharge of a $LiFePO_4$/graphite cell.

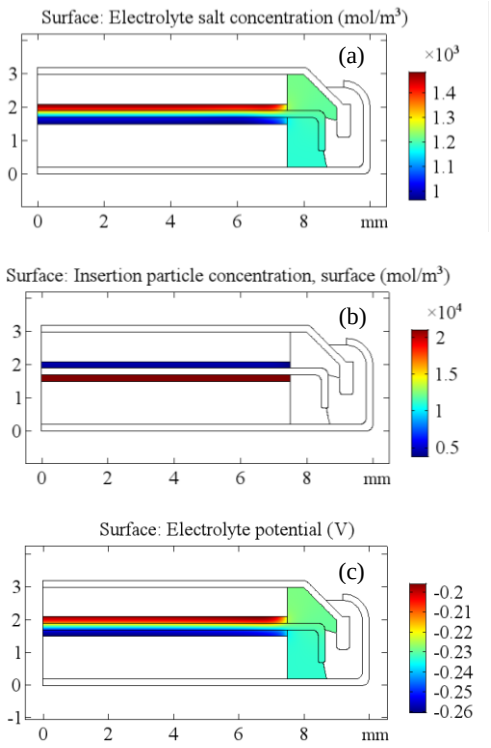

Figure 3. Calculation results of (a) electrolyte salt concentration, (b) lithium concentration at the surface of electrode particles, and (c) electrolyte potential at the end of discharge (C-rate=0.5) for an improved $LiFePO_4$ cathode configuration.

Figure 3 shows the calculation results for an improved $LiFePO_4$ cathode configuration, in which the length of LFP is adjusted to be the same as that of graphite. As a result, the distributions of electrolyte salt concentration and lithium concentration in the electrodes become uniform.

3.2 Discharge characteristics of $LiCoO_2$/ graphite and $LiMn_2O_4$/graphite coin cells

In order to compare $LiFePO_4$ (LFP) cathode with other cathode materials, the discharge characteristics of $LiCoO_2$ (LCO)/graphite and $LiMn_2O_4$ (LMO)/graphite coin cells are also calculated in this work. Since the capacity of LCO cathode is much higher than that of graphite, here we reduce the thickness of LCO to make the capacity of LCO be the same as that of graphite. Results show that the cell voltage of LCO/ graphite decreases fast from 4.1 to 3.4 V, *i.e.*, 17%, and the cell voltage of LMO/graphite decreases a little slow, from 4.0 to 3.6 V, *i.e.*, 10% before depletion. The average SOC of graphite electrode for the $LiCoO_2$ (LCO)/graphite cell decreases from 0.93. This means that the almost full capacity of graphite is used for full charge. The variation of average SOC for the $LiMn_2O_4$ (LMO)/graphite cell is similar to that of LFP.

4. Conclusions

This paper reports the simulation results of a $LiFePO_4$/graphite lithium-ion coin cell battery. It is found that the distributions of lithium ion concentration, potential and lithium concentration at the electrode particles can be improved by adjusting the electrode configuration. At low discharge rates, the decrease of the cell voltage of $LiFePO_4$/graphite before depletion is slower than those of other cathode materials, which would be beneficial in industrial applications of $LiFePO_4$ in near future.

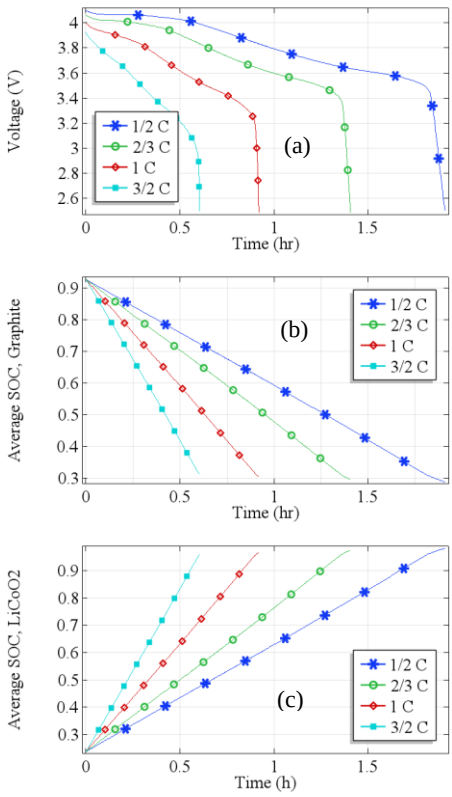

Figure 4. Temporal evolutions of (a) cell voltage, (b) average SOC in graphite electrode, and (c) average SOC in $LiCoO_2$ electrode during the discharge of a $LiCoO_2$/graphite cell.

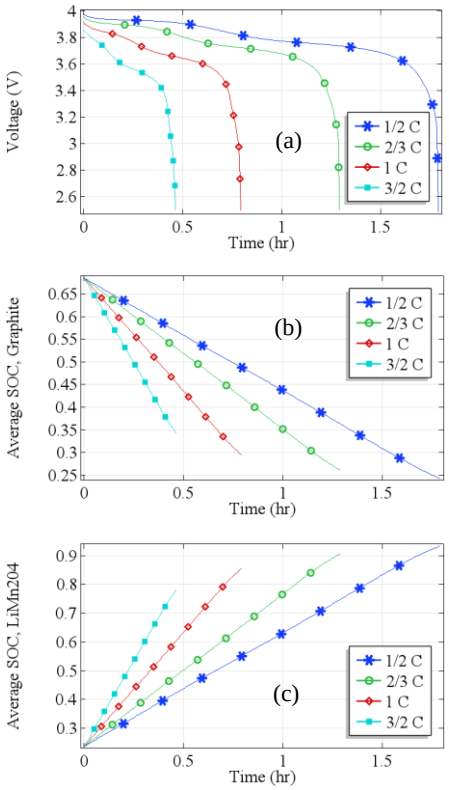

Figure 5. Temporal evolutions of (a) cell voltage, (b) average SOC in graphite electrode, and (c) average SOC in $LiMn_2O_4$ electrode during the discharge of a $LiMn_2O_4$/graphite cell.

5. References

1. L. Zhang, C. Lyu, G. Hinds, L. Wang, W. Luo, J. Zheng, and K. Ma, "Parameter sensitivity analysis of cylindrical $LiFePO_4$ battery performance using multi-physics modeling", *Journal of The Electrochemical Society* **161** (5), A762-A776 (2014).

2. E. Prada, D. Di Domenico, Y. Creff, J. Bernard, V. Sauvant-Moynot, and F. Huet, "Simplified electrochemical and thermal model of $LiFePO_4$-graphite Li-ion batteries for fast charge applications", *Journal of The Electrochemical Society* **159** (9), A1508-A1519 (2012).

3. A. Patil, V. Patil, D. W. Shin, J. W. Choi, D. S. Paik, and S. J. Yoon, "Issue and challenges facing rechargeable thin film lithium batteries", *Materials Research Bulletin* **43**, 1913-1942 (2008).

4. D. H. Doughty and E. P. Roth, "A general discussion of Li ion battery safety", *The Electrochemical Society Interface* **21** (2), *37-44* (2012).

5. A. Melcher, C. Ziebert, M. Rohde, B. Lei, H. J. Seifert, "Modeling and simulation of the thermal runaway in cylindrical 18650 lithium-ion batteries", *The Proceedings of the 2016 COMSOL Conference*, Munich, Oct. 2016.

6. M. Mastali, M. Farkhondeh, S. Farhad, R. A. Fraser, and M. Fowler, "Electrochemical modeling of commercial $LiFePO_4$ and graphite electrodes: kinetic and transport properties and their temperature dependence", *Journal of The Electrochemical Society* **163** (13), A2803-A2816 (2016).

7. D. Li, D. Danilov, Z. Zhang, H. Chen, Y. Yang, and P. H. L. Notten, "Modeling the SEI-formation

on graphite electrodes in $LiFePO_4$ batteries", *Journal of The Electrochemical Society* **162** (6), A858-A869 (2015).
8. V. Srinivasan and J. Newman, "Discharge model for the lithium iron-phosphate electrode", *Journal of The Electrochemical Society* **151** (10), A1517-A1529 (2004).
9. M. Safari, and C. Delacourt, "Modeling of a Commercial Graphite/$LiFePO_4$ Cell", *Journal of The Electrochemical Society* **158** (5), A562-A571 (2011).
10. M. Farkhondeh and C. Delacourt, "Mathematical modeling of commercial $LiFePO_4$ electrodes based on variable solid-state diffusivity", *Journal of The Electrochemical Society* **159** (2), A177-A192 (2012).
11. D. Juarez-Robles, C. F. Chen, Y. Barsukov, and P. P. Mukherjee, "Impedance evolution characteristics in lithium-ion batteries", *Journal of The Electrochemical Society* **164** (4), A837-A847 (2017).
12. M. Safari, and C. Delacourt, "Mathematical modeling of lithium iron phosphate electrode: galvanostatic charge/discharge and path dependence", *Journal of The Electrochemical Society* **158** (2), A63-A73 (2011).
13. R. Ishiguro, S. Nakamura, M. Yoshioka, T. Sakai, T. Mukai, "Practical use technology development of the innovative separator for next-generation lithium ion battery", *Japan Steel Works Technical Review* **66**, 63-72 (2015) [in Japanese].
14. K. E. Thomas, R. M. Darling, J. Newman, "Mathematical modeling of lithium batteries", in *Advances in Lithium-Ion Batteries*, W. A. van Schalkwijk and B. Scrosati, Editors, Kluwer Academic/Plenum Publishers, New York, 345-392 (2002).
15. COMSOL Multiphysics$^{@}$-http://www.comsol.com/products and the Batteries & Fuel Cells Module.